ACS Photonics

Article

Cite This: ACS Photonics 2018, 5, 3159–3165

Room Temperature Electrical Control of Single Photon Sources at 4H-SiC Surface

Shin-ichiro Sato,*[,†] Tomoya Honda,[†,‡] Takahiro Makino,[†] Yasuto Hijikata,[‡] Sang-Yun Lee,[§] and Takeshi Ohshima[†]

[†]Quantum Beam Science Research Directorate, National Institutes for Quantum and Radiological Science and Technology, Takasaki, Gunma 370-1292, Japan

[‡]Graduate School of Science and Engineering, Saitama University, Saitama, 338-8570 Japan

[§]Center for Quantum Information, Korea Institute of Science and Technology, Seoul, 02792, Republic of Korea

ABSTRACT: Single photon source (SPS) providing nonclassical light states on demand is one of the key technologies for the application of quantum communication and optical quantum computer. In this paper, room temperature electrical control of single photon emission from defects at 4H-SiC surface is presented. Planar-type 4H-SiC p^+nn^+ diodes are fabricated and defects that act as SPS are formed on the surface of n-type epi-layer by field oxidation process. The photon emission properties of SPSs are investigated using a home-built confocal microscopy. Results show that the electroluminescence (EL) intensity of SPS can be controlled by minority carrier injection of forward bias voltages, while the photoluminescence (PL) intensity of SPS can be controlled by reverse bias voltages. No significant variations due to applied bias voltages are observed in the EL and PL spectra, indicating the defect structure and charge state are unchanged. The PL intensity modulation by switching a reverse bias voltage is also demonstrated.

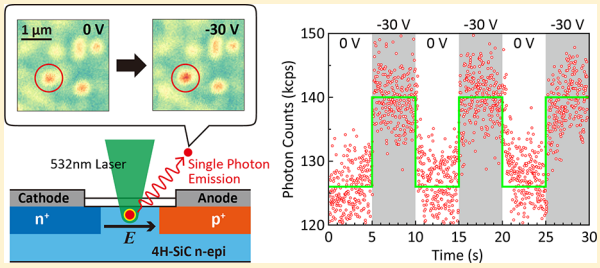

KEYWORDS: *silicon carbide, optically active defects, single photon source, defect engineering, photon emission modulation*

Reliable and efficient single photon sources (SPSs) providing nonclassical light states on demand are of great importance in the fields of quantum computation, communication, and metrology.[1−3] Single photon emission has been observed from a variety of quantum emitters including semiconductor quantum dots,[3−7] molecules,[8] atoms,[9,10] ions,[11] and color centers in wide-bandgap semiconductors. Within these systems, color centers in wide-bandgap semiconductors have especially attracted attention because of their stable luminescence at room temperature (RT) and the potential of installation into electric devices. One of the most outstanding SPSs is nitrogen-vacancy (NV) center in diamond[12] and the electrical excitation at RT of NV^0 (neutrally charged NV) has been demonstrated.[13,14] However, there are limitations of diamond-based electrically driven SPSs at present because of immature fabrication processes of diamond devices.

Optically active defects that behave as SPS, other than NV centers in diamond, have been explored,[15] and silicon carbide (SiC) is one of the promising materials to realize quantum-based devices including electrically driven SPS.[16,17] SiC is a wide-bandgap semiconductor being the most technologically relevant given the ability to grow epitaxially high quality bulk single crystal and films. It is currently commercially available in up to 6 in. wafers and the device engineering technologies are well developed. Recently, several SPSs have been reported in SiC: silicon vacancy (V_{Si}),[18−20] divacancy (V_CV_{Si}),[21,22] carbon antisite-carbon vacancy pair ($C_{Si}V_C$),[23] and so on. Also, ultrabright and fully polarized SPSs (surface SPS) have been found in the vicinity of SiC surface under oxide, and photon emissions from the surface SPS were optically and electrically driven at room temperature.[24−26] The structure of the surface SPS, however, has not been identified, and thus, the formation mechanism has not been clarified yet. Lorhmann et al. demonstrated for the first time that photon emission intensity of the defect in a 4H-SiC pn diode could be modulated by changing forward bias voltage, that is, electroluminescence (EL). In this method, not only the target defect, but also the other defects, like the D1 centers[27−29] show strong photon emissions and this causes the reduction of signal-to-noise ratio of SPS.

Another method to electrically control SPSs is to apply an external electric field to the SPS by means of a reverse bias voltages of diode and to change the charge state of SPS, resulting in the change in intensity of photon emission (photoluminescence: PL).[30] In this paper, we demonstrate the electrical control of PL intensity of the surface SPS in 4H-SiC diode by using reverse bias voltages as well as the electrical control of EL intensity by using forward bias voltages. The possible mechanism of these properties is discussed based on the defect structure that has been proposed.

Received: March 23, 2018
Published: May 23, 2018

DOI: 10.1021/acsphotonics.8b00375
ACS Photonics 2018, 5, 3159–3165

SAMPLE FABRICATION AND CHARACTERIZATION

A schematic drawing of diodes used in this study is shown in Figure 1a. Planar type p^+nn^+ diodes were fabricated on an n-type 4H-SiC epitaxial layer with a donor concentration of 4.7×10^{14} cm^{-3}, which was grown on an n-type 4H-SiC substrate (Si face, 4° off). Phosphorus and aluminum ion implantations at a temperature of 800 °C, followed by thermal annealing at 1800 °C for 10 min in an argon atmosphere were performed to form the n^+- and p^+-type contact regions. The donor and the acceptor concentrations were 2.0×10^{20} cm^{-3} and 5.0×10^{19} cm^{-3}, respectively. A field oxide layer was subsequently formed on the surface by pyrogenic oxidation (H_2/O_2 = 1:1) at the temperature of 1100 °C. The thickness of oxide layer was estimated to be 41 nm. Aluminum electrodes were formed on the n^+- and p^+-type contact regions. The p^+- and n^+-contact regions were designed to be 10 μm wider than Al electrodes in order to avoid misalignment of electrodes during the lithography process. Current−voltage (*IV*) characteristics of the diode are shown in Figure 1b. The ordinate of Figure 1b shows the absolute value of current. The *IV* characteristics under 532 nm laser illumination at 1.0 mW are also illustrated (the detail is explained later). The inset of Figure 1b shows the same data with linear ordinate and the negative sign of current indicates reverse direction from the p^+n junction.

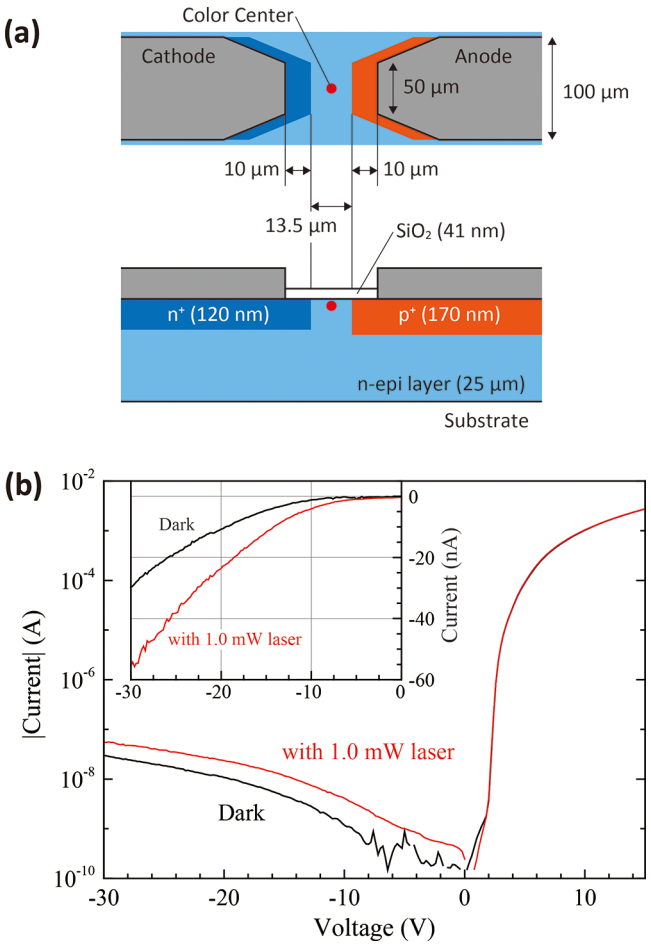

Figure 1. (a) Schematic drawing of planar-type 4H-SiC diode used in this study and (b) the *IV* characteristics under dark conditions (black) and with 532 nm, 1.0 mW laser illumination (red) at room temperature. The ordinate is the absolute value of current. The inset depicts the same data with linear ordinate.

SPSs in the diode, which are formed during the sample fabrication, were investigated by the home-built confocal microscopy (CFM). The diode was connected to the source and measurement unit (Keysight B2911A) to apply bias voltages during the CFM measurement. Luminescence from the SPSs in the diode was collected with a 0.95 N.A. objective lens (OLIMPUS MPLAPON50x) and detected by Si avalanche photodiodes (APDs, LASER COMPONENTS Count-100C). Two APDs were installed in the CFM and antibunched photon emission was confirmed by Hanbury-Brown and Twiss (HBT) interferometry.[31] A 647 nm long pass filter was placed in front of the APDs. Luminescence spectra of SPSs were investigated by an imaging spectrometer (HORIBA iHR320 and Synapse CCD) installed in the CFM. A 561 nm long pass filter was placed in front of the spectrometer.

When a forward bias voltage is applied to the diode, SPSs in the diode emit photons due to carrier injection (EL). No laser excitation was used for the detection of SPSs while forward bias voltages were applied. EL spectra with different bias voltages and the second-order correlation function of SPSs were investigated. On the other hand, a 532 nm laser was used for excitation of surface SPSs (PL) when a reverse bias voltage is applied. The reverse bias voltage was varied and photon emission intensity of SPSs was investigated. All measurements were performed at room temperature (RT).

RESULTS

We first performed wide range CFM scans to observe the whole n-region of diode with different forward bias voltages (EL-CFM). No excitation laser was used when the forward bias voltages were applied. EL intensities for all over the region increased with increasing forward bias voltage. Figure 2a shows EL intensity maps of a region near the p^+n junction with different forward bias voltages (5.0, 7.5, and 10.0 V). The results clearly showed that the EL intensity of the n-region near p^+n junction drastically increased with increasing forward bias voltage. This is because when minority carriers are injected into the n-region by applying a forward bias voltage, injected carriers are trapped and radiatively recombine in color centers.[32] An electron in the ground state of color center is also excited by energy-transfer from nonradiative recombination of carriers and emit photons when the electron is de-excited to the ground state. A color center named "X", which is encircled by a black dashed line in Figure 2a showed strong luminescence, and the EL intensity increased with increasing forward bias voltage, although the EL spectra did not change as shown in Figure 2b. Figure 2c shows the second-order autocorrelation function $g^2(\tau)$ of the color center X at 7.5 V measured by the HBT interferometry. The experimental data were plotted after background correction.[33] In this measurement, $\rho = S/S + B$ was 0.70, where S and B were the signal and the background photon counts, respectively. The value of $g^2(\tau = 0)$ was found to be below 0.5, indicating this color center has single-photon emission characteristics. The antibunching characteristics was not significantly changed due to applied forward bias voltage. Therefore, we conclude from these results that the increase in EL intensity by applied forward bias voltage is attributable to the increase in photon emission intensity of the SPS and electrical control of photon emission from the SPS is successfully demonstrated. The sharp bunching shoulder

DOI: 10.1021/acsphotonics.8b00375
ACS Photonics 2018, 5, 3159−3165

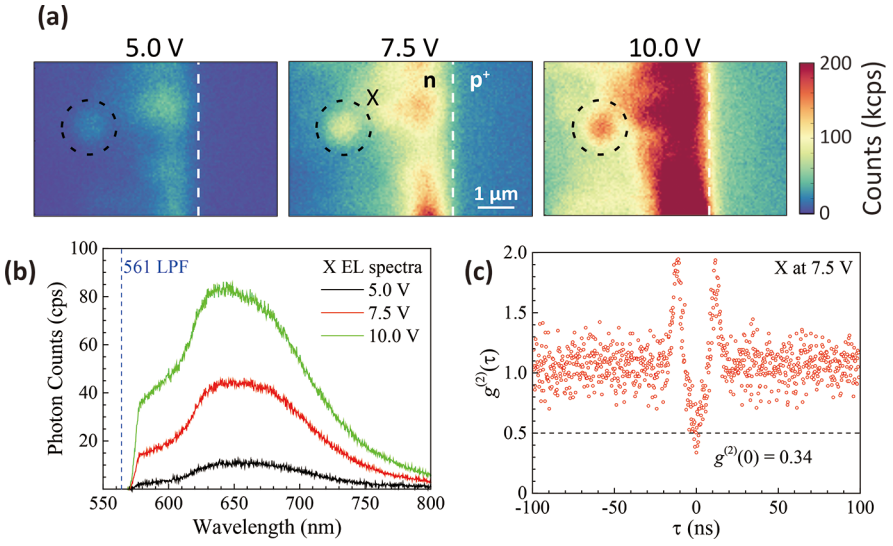

Figure 2. (a) EL-CFM maps with different forward bias voltages. White dashed lines show the boundary between the epi-region (n-region) and the p^+-region. (b) EL spectra of a color center "X" in (a) with different bias voltages. (c) Measurement of the second-order autocorrelation function of the color center "X" at 7.5 V. The uncorrelated background was corrected and the value of $g^{(2)}(0)$ is shown.

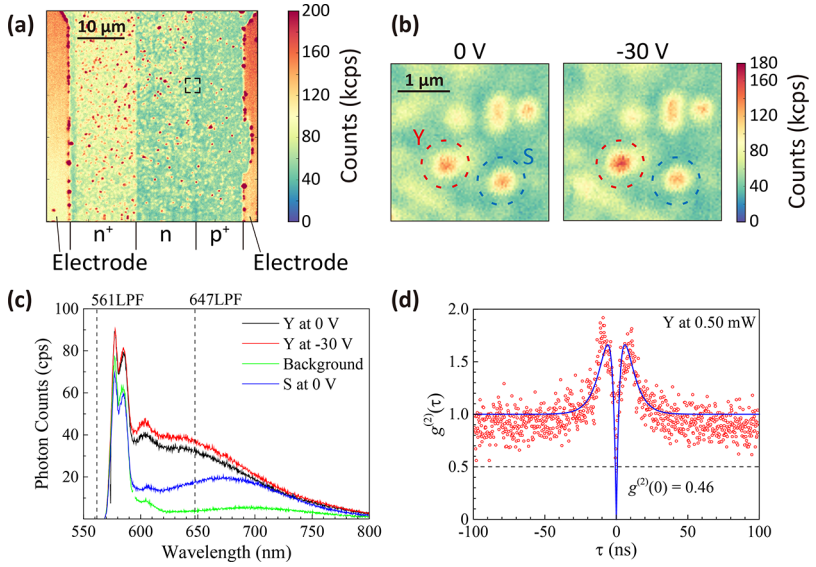

Figure 3. (a) Wide scan PL-CFM map of the diode with 532 nm laser excitation at 1.0 mW. (b) Focused PL-CFM maps without reverse bias voltage (left) and with −30 V (right). The color centers Y and S that, respectively, responded and did not respond to the applied bias voltage are encircled by dashed lines. (c) PL spectra of the color centers Y and S and the background. The strong peaks at around 580 nm are the second order Raman shift. (d) Measurement of the second-order autocorrelation function of the color center Y at 0.5 mW. The uncorrelated background was corrected and the experimental value of $g^{(2)}(0)$ is shown in the figure. The fitting curve by eq 1 is also drawn.

appeared in Figure 2c can be potentially explained by the fast intersystem crossing from and to an intermediate state.

A wide range CFM scan under 532 nm laser excitation at an intensity of 1.0 mW was performed (PL-CFM). The result is shown in Figure 3a. The n^+, n, and p^+ regions, as well as the electrodes, are clearly distinguished, and many bright spots are found in all regions. The overall luminescence intensities in the n^+ region were higher than those in the other regions. This is because the implantation dose of n^+ region was 4× higher than that of p^+ region, and the larger amount of D1 centers still remained even after the thermal annealing at 1800 °C, meaning that the D1 centers were thermally quite stable. On the other hand, ion implantation did not contribute to the formation of color centers in the vicinity of the SiC surface. The D1 centers, one of the popular color centers whose spectral range is 450−650 nm at room temperature, show strong EL.[32] Although the origin of the D1 center is still open to discussion, several models have been proposed, including the bound-exciton-like center[27,28] and the antisite pair (Si_CC_{Si}).[29] The luminescence from D1 centers was regarded as background photon counts, although the color centers were clearly found in any of p^+, n, and n^+ regions.

About 100 color centers in the n region were investigated in terms of the photon emission intensity change due to reverse bias voltage, and as a result, two SPSs (i.e., roughly 2% of color centers) that photon emission intensities responded to reverse bias voltage were found. One of these two SPSs was found at the distance of 1.3 μm from the boundary of the p^+ region, which is shown as the black open square in Figure 3a, and the other was found at the distance of 1.6 μm from the boundary of

DOI: 10.1021/acsphotonics.8b00375
ACS Photonics 2018, 5, 3159−3165

n^+ region (not shown). Hereinafter, the former and latter centers are called as the color centers Y and Z, respectively. Focused CFM scans with different reverse bias voltages are shown in Figure 3b. The intensity of the color center Y clearly increased due to the reverse bias voltage of −30 V, whereas no significant change of the intensity appeared in a color center encircled by the blue dashed line in Figure 3b (color center S). PL spectra of the color centers Y and S are shown in Figure 3c. A strong peak at around 580 nm, which appeared in all the data, is the second order Raman shift,[34] and a small peak at around 600 nm is thought to be an artifact that often appears probably due to the stray light in the measurement setup. As evidence, it shows up in the background spectrum as well. The color center Y shows the broad spectrum of the peak is about 630 nm. The broad PL spectrum originates from the phonon sideband of color center Y and the zero phonon line was not clearly observed at room temperature. The intensity of color center Y simply rose by 11% without change in the spectrum when the reverse bias voltage of −30 V was applied. The color center S also shows the broad spectrum of the peak is about 670 nm, which is longer than the color center Y. The second-order autocorrelation function of the color center Y was measured, and the result is shown in Figure 3d. The value of $\rho = S/S + B$ was 0.68 in this measurement. The value of $g^{(2)}(\tau = 0)$ was found to be below 0.5, indicating the color center showed single-photon emission characteristics. We conclude from these results that the increase in PL intensity of Y by applied reverse bias voltage was attributable to the increase in photon emission from the SPS. Assuming the three level system, the antibunching characteristics can be explained by the double exponential function:

$$g^2(\tau) = 1 - (1 + \alpha)\cdot\exp\left(-\frac{\tau}{\tau_1}\right) + \alpha\cdot\exp\left(-\frac{\tau}{\tau_2}\right) \quad (1)$$

where τ is the delay time. The values of α, τ_1, and τ_2 are fitting parameters relating to the nonradiative decays and transitions via the metastable state, the transition between ground and excited state, and the behavior of the metastable state, respectively.[25] The experimental data was well fitted by eq 1, and the obtained values of α, τ_1, and τ_2 were 3.4, 3.2, and 6.4 ns, respectively. On the other hand, the antibunching characteristics of EL, shown in Figure 2c, were not well fitted by eq 1. This fact is in agreement with the previous literature[24] and suggests that the EL mechanism of surface SPS cannot be simply explained by the three level system and another energy level is involved. However, the PL spectra of color centers Y and S are analogous to the EL spectra of color centers, including X, indicating that these color centers originate from the same types of defects.[24] The difference in wavelength range among these surface SPSs is thought to reflect the difference in lattice strains near the surface SPSs which was introduced by the surface oxidation. The lattice strain affects the energy level of surface SPSs. It should be noted, the result that roughly 2% of color centers responded to reverse bias voltage significantly underestimate the actual situation. Since spatially large and strong luminescence spots found in the wide range CFM scan (see Figure 3a) are thought to be composed of multiple color centers, it would be difficult to find the color center that responds to bias voltages in these spots. In addition, color centers that weakly respond to bias voltages might be overlooked.

In order to demonstrate the electrical control of color centers, we measured the photon count variation of Y by switching the reverse bias voltage. The reverse bias voltage was set to −30 V, and the switching period was 5 s. The result is shown in Figure 4a. The color center Y obviously followed the

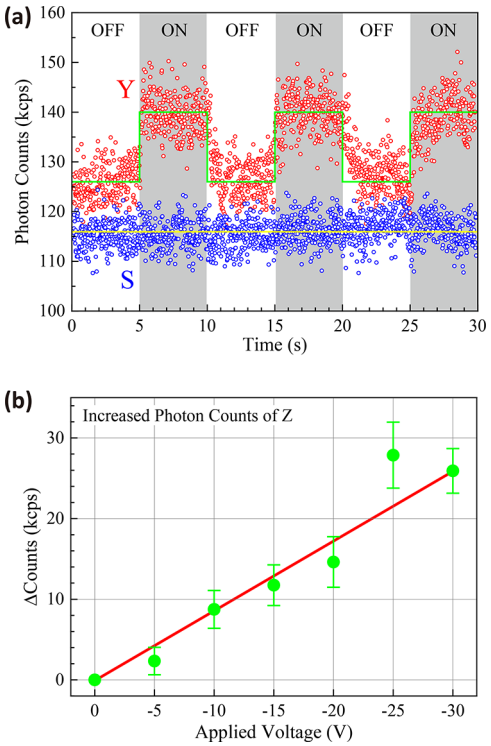

Figure 4. (a) Photon count variations of the color center Y by switching the applied bias voltage. ON and OFF in the figure denote the applied bias voltages were 0 and −30 V, respectively. (b) Increased photon counts of the color center Z with increasing applied reverse bias voltage (averaged values for 5 s). The error bars denote the estimated standard deviations. Lines in (a) and (b) are drawn to guide the eye.

switching and increased the photon counts from 126 to 140 kcps when the switch was ON, although the color center S kept a constant value independent of the switching (116 kcps). In Figure 4b, the photon count variation of the color center Z by changing the applied reverse bias voltages is shown. The ordinate is the increased photon intensity compared to the value without bias voltage and the data were the average values for 5 s. The average photon counts clearly increased with increasing the reverse bias voltage. Interestingly, a jump of experimental data appeared at −25 V, and this phenomenon is thought to be associated with the stability under external electric fields, which is discussed later.

DISCUSSION

We first summarize the candidate of origins of surface SPSs and discuss the mechanism of their electrical control. Several models have been proposed for the origin of surface SPS but no concrete evidence has been obtained. At least primary point defects have been excluded from the origin in previous reports, since they cannot account for the large variance of PL spectra.[24] Lohrmann et al. revealed from polarization behavior of that two dipole orientations appeared from the photon absorption and emission, indicating an alignment of the defect dipoles with the

DOI: 10.1021/acsphotonics.8b00375
ACS Photonics 2018, 5, 3159−3165

cubic lattice.[35] This reported result suggests that surface SPSs are located very near to the SiO_2/SiC interface but in the SiC side. Also, the surface SPS might be attributable to oxygen-related defects. In general, various extended defects such as carrot defects, basal plane Frank-type defects, 3C inclusions, and stacking faults have been observed in 4H-SiC epitaxial layers.[36] Also, SiO_2/SiC interface contains strain because of the lattice mismatch between SiO_2 and SiC. Such imperfection of crystal near surface SPS has the potential to lead to the various ranges of their PL spectra. Tsunemi et al. have reported that there were two types of PL spectra of surface SPSs and the peak wavelength widely varied.[37]

Here we discuss the relationship between the photon emission intensity of surface SPSs and the applied bias voltage based on this defect structure. What should be considered first is the effect of depletion region expanded by reverse bias voltages. The depletion layer of n-region near the boundary of p^+ region expands by reverse bias voltage and SPSs in the depletion region changes their charge state because the energy level of SPS goes below the Fermi level, resulting in the change in photon emission properties. This mechanism has been recently demonstrated by Casas et al.[30] In the case of devices used in this study, the depletion width was calculated from the donor concentration of the n region (4.7×10^{14} cm^{-3}) to be 2.6 μm at 0 V and 8.7 μm at −30 V. If these calculated values were simply accepted, the color center Z located near the boundary of n^+ region would not be depleted and no electric field would be applied even at the bias of −30 V, while the color center Y located near the boundary of p^+ region was depleted without reverse bias voltage. Therefore, the results obtained in this study cannot be accounted for in terms of the expansion of depletion region due to reverse bias voltage only, although we originally expected this mechanism for the electrical control of surface SPSs.

If the color centers Y and Z were located very near the 4H-SiC surface, the effects of 4H-SiC surface and SiO_2/4H-SiC interface should be taken into account. Interface traps in addition to an interfacial layer are present at SiO_2/4H-SiC interface and strongly affect the band structure.[38,39] Watanabe et al. revealed from synchrotron radiation X-ray photoelectron spectroscopy that an upward band bending of 0.10 eV appeared at SiO_2/4H-SiC interface on (0001) Si-face due to carrier compensation of interface traps.[40,41] The interface traps are negatively charged and reduces the net donor concentration near the 4H-SiC surface. The net donor concentration near the interface of our devices was estimated to be 1.0×10^{13} cm^{-3} when the effective density of states in the conduction band was $3.25 \times 10^{15} \times T^{3/2}$ cm^{-3} at $T = 298$ K.[42] In this case, the space charge region (depletion region) is thought to be formed near the surface throughout the whole n region, since the estimated depletion width at the surface exceeds the n region width (13.5 μm). An almost uniform electric field was applied in the vicinity of 4H-SiC surface between the p^+ region and the n^+ region and increase with increasing applied bias voltage. Therefore, the same intensity of electric field should be applied to both the color centers Y and Z, suggesting the enhancement of photon emission intensity was induced by the same mechanism. We believe these color centers were located at a region less than several nm from the interface, although it is difficult to estimate the exact distance at present stage.

Next, behaviors of photoexcited carriers around the surface SPS is discussed. When the SPS is continuously excited by 532 nm laser and emits photons, electron−hole (*e*-*h*) pairs are also generated within the bandgap and are observed as the photoinduced current of the device. Although the photon energy of 532 nm wavelength (2.33 eV) is lower than the bandgap of 4H-SiC (3.26 eV), electrons in the valence band can be excited to the conduction band via localized defect levels. According to the result of *IV* characteristics under 532 nm laser illumination, as shown in Figure 1b, the photocurrent of 25 nA were generated at the bias voltage of −30 V. Note that the *IV* measurement was performed at the CFM setup and the condition was exactly the same with the experiment for the bias voltage response of SPS. Assuming no carrier recombination occurred during the diffusion process, the number of generated *e*-*h* pairs were calculated to be 1.6×10^{11} carriers/s. Thus, the local carrier density around the laser illuminated area was roughly estimated to be 1.3×10^{18} cm^{-3} by using the carrier lifetime of 2.0 μs[43] and the volume of 2.5×10^{-13} cm^3 determined from the objective lens and the laser wavelength. It is obvious from this approximate calculation that the (quasi) Fermi level at around the surface SPSs during laser illumination was unchanged by reverse bias voltages, since the laser-induced carriers (1.3×10^{18} cm^{-3}) were far higher than the net donor concentration (1.0×10^{13} cm^{-3}). We conclude therefore that the photon emission enhancement of color centers Y and Z is not attributable to the change in charge state, as reported for divacancies.[30]

The fact of the photon emission enhancement without changes in PL spectra suggests that the radiative transition rate of surface SPS simply increased and/or the transition rate to "dark states" decreased. If the origin is a defect embedded in 3C inclusion, quantum confinement of 3C inclusion might affect the photon emission properties of surface SPS. The growth of multiquantum well (QW) structure of SiC which consists of 3C-SiC wells and 4H-SiC barriers has been demonstrated.[44,45] Since 3C inclusions of width less than 10 nm in 4H-SiC could show the properties of QW at room temperature,[44] it is likely that an electron at the excited state of surface SPS is also photoexcited to the quantum level of 3C inclusion and this excitation process decreases the radiative transition rate of surface SPS. An electron at the quantum level will thermally escape or radiatively recombine to hole in the valence band. When an electric field is applied to QW of 3C inclusion, the quantum confinement Stark effect[46] appears, and as a result, the red shift of quantum level and the lifetime extension of radiative recombination occurs. These effects are a consequence of the QW potential that reduces the exciton biding energy and separates electrons from holes.[47,48] The lifetime extension (in other words, decrease in transition rate) of QW level of 3C inclusion drastically increase with increasing the QW width[49] and probably provides the increase in radiative transition rate of surface SPS. Therefore, the surface SPSs which respond to reverse bias voltages (color centers Y and Z) are likely to be attributed to a defect embedded in a large size of 3C inclusion. We anticipate that multiple dark states including the QW level of 3C inclusion would affect the photon emission properties of surface SPSs.

Finally the stability of photon emission of SPSs is discussed. We observed a clear difference of stability between the color centers Y and Z. "Blinking" of photon emission was observed in the color center Z, whereas the color center Y were quite stable for a prolonged period of time (about 2 h). The photon emission intensity of color center Z gradually became unstable during the measurement and eventually lost the response to bias voltages. The reason the value of −30 V is lower than −25

DOI: 10.1021/acsphotonics.8b00375
ACS Photonics 2018, 5, 3159−3165

V in Figure 4(b) is thought to be due to the blinking of color center Z. However, the photon emission intensity of color center Z again responded to bias voltages another day, indicating the factor(s) affecting the blinking is of reversible nature. Additional theoretical and experimental studies are required to clarify the mechanism of these properties as well as the exact defect structure of surface SPS.

SUMMARY

We fabricated the planar-type 4H-SiC p^+nn^+ diodes and demonstrated the electrical control of surface SPSs at RT which were formed in the vicinity of the surface of 4H-SiC during the device fabrication. First we demonstrated the control of surface SPS by means of minority carrier injection by applying forward bias voltages. The photon emission intensity increased with increasing forward bias voltage without changes in EL spectra. Also, we investigated the PL intensity variations of surface SPSs induced by reverse bias voltages and found two SPSs showed the photon emission enhancement without changes in PL spectra.

AUTHOR INFORMATION

Corresponding Author

*E-mail: sato.shinichiro2@qst.go.jp.

ORCID

Shin-ichiro Sato: 0000-0001-9359-9400

Yasuto Hijikata: 0000-0002-6314-0401

Takeshi Ohshima: 0000-0002-7850-3164

Author Contributions

T.O. proposed the idea. T.O. and Y.H. designed the experiment. T.H. and S.S. performed the experiment and analyzed the data. S.Y.L. and T.O. designed the device. T.H., T.M., and T.O. fabricated the devices. S.S. prepared the manuscript. T.H. and S.S. contributed equally to this work. All authors discussed the results and contributed to the manuscript.

Notes

The authors declare no competing financial interest.

ACKNOWLEDGMENTS

This study was supported by JSPS KAKENHI (17H01056 and 26286047) and Iketani Science and Technology Foundation (0291081-A). We would like to express our gratitude to Dr. Hidekazu Tsuchida and Dr. Norihiro Hoshino of Central Research Institute of Electric Power Industry (CRIEPI) who provided the epitaxial substrate used in this study. We also would like to thank Dr. Brett. C. Johnson and A/Prof. Jeffrey C. McCallum of the University of Melbourne for fruitful discussions.

REFERENCES

(1) Lounis, B.; Orrit, M. Single-photon sources. *Rep. Prog. Phys.* **2005**, *68*, 1129−1179.

(2) Boretti, A.; Rosa, L.; Mackie, A.; Castelletto, S. Electrically driven quantum light sources. *Adv. Opt. Mater.* **2015**, *3*, 1012−1033.

(3) Lohrmann, A.; Johnson, B. C.; McCallum, J. C.; Castelletto, S. A review on single photon sources in silicon carbide,. *Rep. Prog. Phys.* **2017**, *80*, 034502−1−23.

(4) Santori, C.; Fattal, D.; Vučković, J.; Solomon, G. S.; Yamamoto, Y. Indistinguishable photons from a single-photon device. *Nature* **2002**, *419*, 594−597.

(5) Michler, P.; Kiraz, A.; Becher, C.; Schoenfeld, W. V.; Petroff, P. M.; Zhang, L.; Hu, E.; Imamogùlu, A. A Quantum Dot Single-Photon Turnstile Device. *Science* **2000**, *290*, 2282−2285.

(6) Yuan, Z.; Kardynal, B. E.; Stevenson, R. M.; Shields, A. J.; Lobo, C. J.; Cooper, K.; Beattie, N. S.; Ritchie, D. A.; Pepper, M. Electrically Driven Single-Photon Source. *Science* **2002**, *295*, 102−105.

(7) Awschalom, D. D.; Bassett, L. C.; Dzurak, A. S.; Hu, E. L.; Petta, J. R. Quantum Spintronics: Engineering and Manipulating Atom-Like Spins in Semiconductors. *Science* **2013**, *339*, 1174−1179.

(8) Nothaft, M.; Hföhla, S.; Jelezko, F.; Frühauf, N.; Pflaum, J.; Wrachtrup, J. Electrically driven photon antibunching from a single molecule at room temperature. *Nat. Commun.* **2012**, *3* (628), 1−6.

(9) McKeever, J.; Boca, A.; Boozer, A. D.; Miller, R.; Buck, J. R.; Kuzmich, A.; Kimble, H. J. Deterministic Generation of Single Photons from One Atom Trapped in a Cavity. *Science* **2004**, *303*, 1992−1994.

(10) Kuhn, A.; Hennrich, M.; Rempe, G. Deterministic Single-Photon Source for Distributed Quantum Networking. *Phys. Rev. Lett.* **2002**, *89*, 067901.

(11) Keller, M.; Lange, B.; Hayasaka, K.; Lange, W.; Walther, H. Continuous generation of single photons with controlled waveform in an ion-trap cavity system. *Nature* **2004**, *431*, 1075−1078.

(12) Wrachtrup, J.; Jelezko, F. Processing quantum information in diamond. *J. Phys.: Condens. Matter* **2006**, *18*, S807−S824.

(13) Lohrmann, A.; Pezzagna, S.; Dobrinets, I.; Spinichelli, P.; Jaxques, V.; Roch, J.-F.; Meijer, J.; Zaitsev, A. M. Diamond based light-emitting diode for visible single-photon emission at room temperature. *Appl. Phys. Lett.* **2011**, *99*, 251106.

(14) Mizuochi, N.; Makino, T.; Kato, H.; Takeuchi, D.; Ogura, M.; Okushi, H.; Nothaft, M.; Neumann, P.; Gali, A.; Jelezko, F.; Wrachtrup, J.; Yamasaki, S. Electrically driven single-photon source at room temperature in diamond. *Nat. Photonics* **2012**, *6*, 299−303.

(15) Neitzke, O.; Morfa, A.; Wolters, J.; Schell, A. W.; Kewes, G.; Benson, O. Investigation of Line Width Narrowing and Spectral Jumps of Single Stable Defect Centers in ZnO at Cryogenic Tempertaure. *Nano Lett.* **2015**, *15*, 3024−3029.

(16) Castelletto, S.; Johnson, B. C.; Boretti, A. Quantum Efects in Silicon Carbide Hold Promise for Novel Integrated Devices and Sensors. *Adv. Opt. Mater.* **2013**, *1*, 609−625.

(17) Boretti, A.; Rosa, L. Latest Advances in the Generation of Single Photons in Silicon Carbide. *Technologies* **2016**, *4*, 16−1−6.

(18) Ivády, V.; Davidsson, J.; Son, N. T.; Ohshima, T.; Abrikosov, I.; Gali, A. Identification of Si-vacancy related room-temperature qubits in 4*H* silicon carbide. *Phys. Rev. B: Condens. Matter Mater. Phys.* **2017**, *96*, 161114−1−5.

(19) Widmann, M.; Lee, S.-Y.; Redler, T.; Son, N. T.; Fedder, H.; Paik, S.; Yang, L.-P.; Zhao, N.; Yang, S.; Booker, I.; Denisenko, A.; Jamali, M.; Momenzadeh, S. A.; Gerhardt, I.; Ohshima, T.; Gali, A.; Janzén, E.; Wrachtrup, J. Coherent control of single spins in silicon carbide at room temperature. *Nat. Mater.* **2015**, *14*, 164−168.

(20) Kraus, H.; Simin, D.; Kasper, C.; Suda, Y.; Kawabata, S.; Kada, W.; Honda, T.; Hijikata, Y.; Ohshima, T.; Dyakonov, V.; Astakhov, G. V. Three-Dimensional Proton Beam Writing of Optically Active Coherent Vacancy Spins in Silicon Carbide. *Nano Lett.* **2017**, *17*, 2865−2870.

(21) Christle, D. J.; Falk, A. L.; Andrich, P.; Klimov, P. V.; Hassan, J. U.; Son, N. T.; Janzén, E.; Ohshima, T.; Awschalom, D. D. Isolated electron spins in silicon carbide with millisecond coherence times. *Nat. Mater.* **2015**, *14*, 160−163.

(22) Christle, D. J.; Klimov, P. V.; Casas, C. F.; Szász, K.; Ivády, V.; Jokubavicius, V.; Hassan, J. U.; Syväjärvi, M.; Koehl, W. F.; Ohshima, T.; Son, N. T.; Janzén, E.; Gali, A.; Awschalom, D. D. Isolated Spin Qubits in SiC with High-Fidelity Infrared Spin-to-Photon Interface. *Phys. Rev. X* **2017**, *7*, 021046.

(23) Castelletto, S.; Johnson, B. C.; Ivády, V.; Stavrias, N.; Umeda, T.; Gali, A.; Ohshima, T. A silicon carbide room-temperature single-photon source,. *Nat. Mater.* **2014**, *13*, 151−156.

(24) Lohrmann, A.; Iwamoto, N.; Bodrog, Z.; Castelletto, S.; Ohshima, T.; Karle, T. J.; Gali, A.; Prawer, S.; McCallum, J. C.; Johnson, B. C. Single-photon emitting diode in silicon carbide. *Nat. Commun.* **2015**, *6*, 7783.

DOI: 10.1021/acsphotonics.8b00375
ACS Photonics 2018, 5, 3159−3165

(25) Lienhard, B.; Schröder, T.; Mouradian, S.; Dolde, F.; Tran, T. T.; Aharonovich, I.; Englund, D. Bright and photostable single-photon emitter in silicon carbide. *Optica* **2016**, *3*, 768−774.
(26) Abe, Y.; Umeda, T.; Okamoto, M.; Kosugi, R.; Harada, S.; Haruyama, M.; Kada, W.; Hanaizumi, O.; Onoda, S.; Ohshima, T. Single photon sources, in 4H-SiC metal-oxide-semiconductor field-effect transistors. *Appl. Phys. Lett.* **2018**, *112*, 031105−1−5.
(27) Fissel, A.; Richter, W.; Furthmüller, J.; Bechstedt, F. On the nature of the D_1-defect center in SiC: A photoluminescence study of layers grown by solid-source modecular-beam epitaxy,. *Appl. Phys. Lett.* **2001**, *78*, 2512−2514.
(28) Egilsson, T.; Bergman, J. P.; Ivanov, I. G.; Henry, A.; Janzén, E. Properties of the D_1 bound exciton in 4H-SiC. *Phys. Rev. B: Condens. Matter Mater. Phys.* **1999**, *59*, 1956−1962.
(29) Gali, A.; Deák, P.; Rauls, E.; Son, N. T.; Ivanov, I. G.; Carlsson, F. H. C.; Janzén, E.; Choyke, W. J. Correlation between the antisite pair and the D_1 center in SiC. *Phys. Rev. B: Condens. Matter Mater. Phys.* **2003**, *67*, 155203−1−5.
(30) Casas, C. F.; Christle, D. J.; Hassan, J. U.; Ohshima, T.; Son, N. T.; Awschalom, D. D. Stark tuning and electrical charge state control of single divacancies in silicon carbide. *Appl. Phys. Lett.* **2017**, *111*, 262403.
(31) Hanbury Brown, R.; Twiss, R. Q. Correlation between photons in two coherent beams of light. *Nature* **1956**, *177*, 27−29.
(32) Fuchs, F.; Soltamov, V. A.; Väth, S.; Baranov, P. G.; Mokhov, E. N.; Astakhov, G. V.; Dyakonov, V. Silicon carbide light-emitting diode as a prospective room temperature source for single photons. *Sci. Rep.* **2013**, *3*, 1637.
(33) Beveratos, A.; Kuhn, S.; Brouri, R.; Gacoin, T.; Poizat, J.-P.; Grangier, P. Room temperature stable single-photon-source. *Eur. Phys. J. D* **2002**, *18*, 191−196.
(34) Burton, J. C.; Sun, L.; Long, F. H.; Feng, Z. C.; Ferguson, I. T. First- and second-order Raman scattering from semi-insulating 4H-SiC. *Phys. Rev. B: Condens. Matter Mater. Phys.* **1999**, *59*, 7282−7284.
(35) Lohrmann, A.; Castelletto, S.; Klein, J. R.; Ohshima, T.; Bosi, M.; Negri, M.; Lau, D. W. M.; Gibson, B. C.; Prawer, S.; McCallum, J. C.; Johnson, B. C. Activation and control of visible single defects in 4H-, 6H-, and 3C-SiC by oxidation. *Appl. Phys. Lett.* **2016**, *108*, 021107−1−4.
(36) Tsuchida, H.; Ito, M.; Kamata, I.; Nagano, M. Formation of extended defects in 4H-SiC epitaxial growth and development of a fast growth technique. *Phys. Status Solidi B* **2009**, *246*, 1553−1568.
(37) Tsunemi, H.; Honda, T.; Makino, T.; Onoda, S.; Sato, S.-I.; Hijikata, Y.; Ohshima, T. Various Single Photon Sources Observed in SiC pin Diodes. *Mater. Sci. Forum* **2018**, na.
(38) Kimoto, T.; Kanzaki, Y.; Noborio, M.; Kawano, H.; Matsunami, H. Interface Properties of Metal−Oxide−Semiconductor Structures on 4H-SiC{0001} and $(11\bar{2}0)$ Formed by N_2O Oxidation. *Jpn. J. Appl. Phys.* **2005**, *44*, 1213−1218.
(39) Afanas'ev, V. V.; Stesmans, A.; Bassler, M.; Pensl, G.; Schulz, M. J. Shallow electron traps at the 4H-SiC/SiO_2 interface. *Appl. Phys. Lett.* **2000**, *76*, 336−338.
(40) Watanabe, H.; Kirino, T.; Kagei, Y.; Harries, J.; Yoshigoe, A.; Teraoka, Y.; Mitani, S.; Teraoka, Y.; Mitani, S.; Nakano, Y.; Nakamura, T.; Hosoi, T.; Shimura, T. Energy Band Structure of SiO_2/4H-SiC Interfaces and its Modulation Induced by Intrinsic and Extrinsic Interface Charge Transfer. *Mater. Sci. Forum* **2011**, *679−680*, 386−389.
(41) Watanabe, H.; Kirino, T.; Kagei, Y.; Uenishi, Y.; Chanthaphan, A.; Yoshigoe, A.; Teraoka, Y.; Shimura, T. Synchrotoron x-ray photoelectron spectroscopy study on thermally grown SiO_2/4H-SiC(0001) interface and its correlation with electrical properties. *Appl. Phys. Lett.* **2011**, *99*, 021907.
(42) Casady, J. B.; Johnson, R. W. Status of silicon carbide (SiC) as a wide-bandgap semiconductor for high-temperature applications: A review,. *Solid-State Electron.* **1996**, *39*, 1409−1422.
(43) Miyazawa, T.; Tsuchida, H. Point defect reduction and carrier lifetime improvement of Si- and C-face 4H-SiC epilayers. *J. Appl. Phys.* **2013**, *113*, 083714−1−6.
(44) Fissel, A.; Kaiser, U.; Schröter, B.; Ritchter, W.; Bechstedt, F. MBE growth and properties of SiC multi-quantum well structures. *Appl. Surf. Sci.* **2001**, *184*, 37−42.
(45) Bai, S.; Devaty, R. P.; Choike, W. J.; Kaiser, U.; Wagner, G.; MacMillan, M. F. Determination of the electric field in 4H/3C/4H-SiC quantum wells due to spontaneous polarization in the 4H-SiC matrix. *Appl. Phys. Lett.* **2003**, *83*, 3171−3173.
(46) Miller, D. A. B.; Chemla, D. S.; Damen, T. C.; Gossard, A. C.; Wiegmann, W.; Wood, T. H.; Burrus, C. A. Electric field dependence of optical absorption near the band gap of quantum-well structures. *Phys. Rev. B: Condens. Matter Mater. Phys.* **1985**, *32*, 1043−1060.
(47) Bastard, G.; Mendez, E. E.; Chang, L. L.; Esaki, L. Variational calculations on a quantum well in an electric field. *Phys. Rev. B: Condens. Matter Mater. Phys.* **1983**, *28*, 3241−3245.
(48) Plentz, F.; Heiman, D.; Pinczuk, A.; Pfeiffer, L. N.; West, K. W. Electron-hole separation in a two-dimensional electron system induced by electric fields. *Solid State Commun.* **1997**, *101*, 103−107.
(49) Köhler, K.; Polland, H.-J.; Schultheis, L.; Tu, C. W. Photoluminescence of two-dimensional excitons in an electric field: Lifetime enhancement and field ionization in GaAs quantum wells. *Phys. Rev. B: Condens. Matter Mater. Phys.* **1988**, *38*, 5496−5503.

DOI: 10.1021/acsphotonics.8b00375
ACS Photonics 2018, 5, 3159−3165